X-ray photoelectron spectroscopy study of the skutterudites $LaFe_4Sb_{12}$, $CeFe_4Sb_{12}$, $CoSb_3$, and CoP_3

Andrew P. Grosvenor,* Ronald G. Cavell, and Arthur Mar
Department of Chemistry, University of Alberta, Edmonton, Alberta T6G 2G2, Canada
(Received 14 April 2006; published 11 September 2006)

The electronic structure of the skutterudites $CoSb_3$, CoP_3, $LaFe_4Sb_{12}$, and $CeFe_4Sb_{12}$ has been investigated with x-ray photoelectron spectroscopy. The binding energies in the pnicogen and transition metal $2p$ spectra are shifted to reflect changes in the bonding character of these compounds. The asymmetric line shapes in the metal $2p$ spectra signal electronic delocalization. A plasmon loss satellite peak occurs in the Co $2p$ spectra of $CoSb_3$ and CoP_3. The intensity of this peak in these and other Co-containing compounds increases with greater occupancy of the Co $3d$ band. The presence of trivalent rare earth was confirmed from the La and Ce $3d$ spectra, both of which contain shake-up satellite peaks. A second satellite peak, attributable to two-core-hole processes, also appears in the La $3d$ spectrum of $LaFe_4Sb_{12}$ but not in $LaFe_4P_{12}$, indicating the involvement of La-Sb covalent bonding and the population of La $4f$ conduction states in the former. This peak is absent in the Ce $3d$ spectrum of $CeFe_4Sb_{12}$ because a $4f^1$ state is located below the Fermi edge. Fitting of the valence band spectra for all four compounds led to the formulations $(Co^{3+})(Pn^{1-})_3$ and $(R^{3+})(Fe^{2+})_4(Sb^{1-})_{12}$, with the electron deficiency in the rare-earth containing compounds being represented by a hole in the valence band.

DOI: 10.1103/PhysRevB.74.125102 PACS number(s): 79.60.−i, 71.20.Lp, 71.45.Gm, 73.20.At

I. INTRODUCTION

The skutterudites represent an extensive class of compounds that originally referred to binary transition-metal pnictides MPn_3 (M=Co, Rh, Ir; Pn=P, As, Sb) that adopt the same structure as the mineral $CoAs_3$.[1,2] Jeitschko and Braun later extended them to include the ternary rare-earth-filled derivatives RM_4Pn_{12} (R=rare earth; M=Fe, Ru, Os; Pn=P, As, Sb).[3–5] In their cubic crystal structure, corner-sharing M-centered octahedra are tilted to form nearly square Pn_4 rings and large dodecahedral voids that are filled by R atoms in the ternary derivatives (Fig. 1). These compounds, especially the antimonides, are most widely acclaimed for their promise as improved thermoelectric materials, which require the incongruous alliance of good electrical conductivity and poor thermal conductivity.[6,7] Unfilled variants, such as $CoSb_3$, were initially targeted as candidates, but attention has shifted to the filled variants, such as $La(Fe_3Co)Sb_{12}$, because of the realization that the thermal conductivity could be reduced further by addition of R.[8]

These compounds are interesting in their own right given the wealth of unusual transport and magnetic properties displayed.[9] In early bonding considerations, the binaries MPn_3 were predicted to be diamagnetic semiconductors, in accordance with a formulation involving low-spin octahedral M^{3+} ($t_{2g}^6e_g^0$) and closed-shell Pn^{1-} species each engaged in two 2 center −2 electron ($2c-2e^-$) Pn-Pn bonds.[3,10] Experimental and theoretical studies generally indicated the existence of a very narrow to zero band gap, but these conclusions were not always definitive.[10–20] For CoP_3, a band gap was suggested from electrical and optical measurements,[10] but there is disagreement among calculations.[13,15,16] For $CoSb_3$, there seems to be consensus that it behaves as a narrow gap semiconductor.[10,12,14,18,20] The simple bonding arguments can be extended to the ternary skutterudites such as RFe_4P_{12}. Because they have fewer valence electrons compared to the previous binaries to achieve a closed-shell configuration, these ternaries were suggested to be hole doped and to contain mixed-valent Fe atoms, in accordance with the formulation $R^{3+}[Fe_4P_{12}]^{3-}$.[3] However, the presence of exclusively low-spin Fe^{2+} in RFe_4Pn_{12} (including $CeFe_4Sb_{12}$) has since been supported by magnetic measurements, Mössbauer spectroscopy, theoretical calculations, and recently, an XPS study.[11,21–23] Most RM_4Pn_{12} compounds are metallic but a few are small band gap semiconductors.[7–9,11,15,24–33] Notably, the semiconducting behavior of $CeFe_4P_{12}$ was initially attributed to the presence of Ce^{4+}, rendering the $[Fe_4P_{12}]^{4-}$ framework isoelectronic to binaries such as CoP_3.[3] However, a trivalent cerium state ($4f^1$) has since been implicated by numerous investigations of $CeFe_4Pn_{12}$ including $CeFe_4Sb_{12}$ which is discussed in this report.[23,26,28,29,34–36]

We have recently applied high-resolution x-ray photoelectron spectroscopy to resolve some of the ambiguities about the electronic structure of these skutterudites, beginning with the rare-earth-filled phosphides $LaFe_4P_{12}$ and $CeFe_4P_{12}$.[23] The interpretation of XPS spectra of intermetallic compounds, especially those containing heavier elements such as the rare earths, is still not well developed. Although these phosphides do not represent practical candidates for thermoelectric materials, they were chosen for the initial study to establish a point of reference for assigning valence states. In the more relevant antimonides RFe_4Sb_{12}, electronegativity differences are smaller and the interpretation of XPS spectra was anticipated to be considerably more challenging.

Here we present detailed interpretations of the XPS spectra of $LaFe_4Sb_{12}$, $CeFe_4Sb_{12}$, $CoSb_3$, and CoP_3. Both high-resolution core-line spectra and valence band spectra are examined with an aim to determine atomic charges and to understand how the nature of bonding differs between the phosphides and antimonides. Although XPS measurements of $CoSb_3$ have been recently reported,[17] no remarks were offered on the distinctive satellite structure that appears in its Co $2p_{3/2}$ spectrum. We suggest an explanation for this feature and we demonstrate how it can be related to the popu-

lation of Co states within the valence band across a series of Co-containing compounds. With the aid of calculated band structures, we attempt to fit the valence band spectra of these antimonide skutterudites through a procedure that we have previously developed for transition-metal phosphides,[23,37] showing that the experimental analysis of the electronic structure of intermetallic compounds with small electronegativity differences can be performed.

II. EXPERIMENTAL SECTION

A. Synthesis

Starting materials were powders of La (99.9%, Alfa-Aesar), Ce (99.9%, Cerac), Fe (99.9%, Cerac), Co (99.999%, Spex), Sb (99.999%, Alfa-Aesar), and P (99.995%, Cerac). Stoichiometric mixtures of the elements were placed in fused-silica tubes that were carbon coated through pyrolysis of acetone. This treatment helps minimize adventitious reactions of the active metals with the silica tube. Sample purity was assessed from powder x-ray diffraction (XRD) patterns collected on an Inel diffractometer equipped with a CPS 120 detector.

Samples of $LaFe_4Sb_{12}$ and $CeFe_4Sb_{12}$ were prepared according to an optimized heating program reported previously.[7] The tubes were heated to 600 °C over 10 h and held there for 3 h, heated to 1050 °C over 12 h and held there for >40 h, and quenched in water. Further annealing at 700 °C for >30 h resulted in high-purity products, with only trace amounts of $FeSb_2$. Samples of $CoSb_3$ and CoP_3 were prepared in the presence of a few grains of iodine. The tubes were heated to 750 °C over 30 h and held at this temperature for 1 week, and then quenched in water. Only trace amounts of unreacted pnicogen were detected in the products. Although air stable, all compounds were stored in a glove box under Ar to preserve pristine surfaces for XPS analysis.

B. XPS analysis

All measurements were performed on a Kratos AXIS 165 spectrometer with a monochromatic Al Kα x-ray source and a base pressure in the analytical chamber of 10^{-6}–10^{-7} Pa. The angle between the x-ray source and the hemispherical analyzer was 54.7°. The resolution function of this instrument has been determined to be 0.4–0.5 eV on the basis of analysis of the Co and Fe Fermi edges.

Samples of $LaFe_4Sb_{12}$, $CeFe_4Sb_{12}$, $CoSb_3$, and CoP_3 were ground under Ar and pressed onto In foil before being transferred to the instrument under Ar to reduce surface oxidation. They were sputter cleaned for nearly 1 h with an Ar^+ ion beam (4 kV, 10 mA) to remove surface contaminants (e.g., C, O, I). Spectra collected throughout the sputter-cleaning process showed no changes except for reduction of the amount of surface oxide, confirming that the sputtering process did not appreciably alter the composition of the studied compounds. For example, the Co:Sb ratio in $CoSb_3$ determined by analysis of survey spectra was 1:2.5 before sputtering and 1:3.1 after sputtering was complete. High-resolution spectra (La, Ce 3*d*; Fe 2*p*; Co 2*p*; Sb 3*d*; P 2*p*; valence band) were then collected with energy envelopes ranging from 60 to 20 eV, a step size of 0.05 eV, a pass energy of 20 eV, a sweep time of 180 s, and an analysis spot size of 700×400 μm. Because these compounds are electrically conducting, charge neutralization was not required during the spectroscopic measurements and charge correction was not applied in the data analysis. The C 1*s* binding energy from adventitious C was equal to the accepted value of 284.8 eV throughout, indicating that charging was not a factor. All results were analyzed with use of the CasaXPS software package.[38] To fit these high-resolution spectra, a Shirley-type function was used to remove the background, which arises largely from inelastic electron scattering. The extracted spectra were then fitted with a combined Gaussian

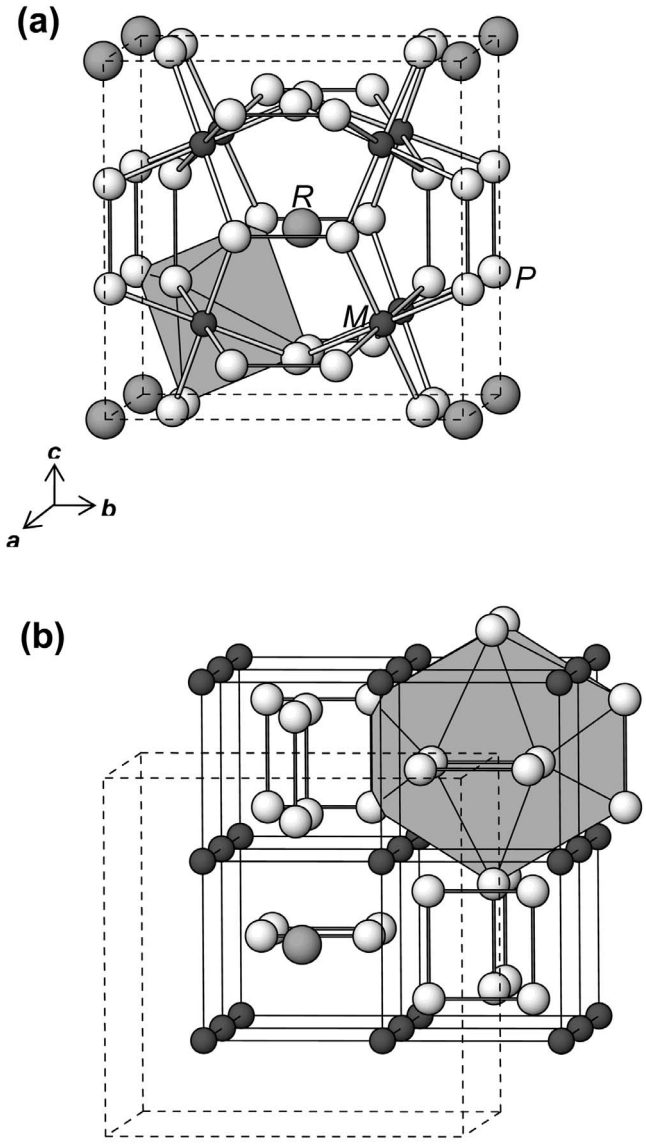

FIG. 1. Filled skutterudite-type structure of ternary rare-earth transition-metal pnictides RM_4Pn_{12}, with the body-centered cubic unit cell outlined in dashed lines. The large gray spheres are *R* atoms, the small solid spheres are *M* atoms, and the medium lightly-shaded spheres are *Pn* atoms. (a) The framework of *M*-centered octahedra is emphasized. (b) An alternative representation highlights the cubic arrangement of *M* atoms enclosing the *R* atoms (centered in a dodecahedral cage) and Pn_4 rings.

(70%) and Lorentzian (30%) line profile to account for spectrometer and life-time broadening, respectively. The Sb 3*d* spectra of the $R\mathrm{Fe_4Sb_{12}}$ compounds indicated the presence of a small amount of Sb oxide that was not removed by Ar^+ sputtering, and the *Pn* spectra of $\mathrm{Co}Pn_3$ indicated the presence of a small amount of oxidized Sb or unreacted P.

C. Band structure calculations

To examine the bonding and distribution of states within the valence band, an extended Hückel tight-binding band structure calculation was performed for $\mathrm{CoP_3}$ with 125 *k* points in the irreducible portion of the Brillouin zone with use of the EHMACC suite of programs.[39,40] The atomic parameters [valence shell ionization potentials H_{ii} (eV) and orbital exponents ζ_i] were as follows. For Co 4*s*, $H_{ii}=-7.8$, $\zeta_i=2.0$; for Co 4*p*, $H_{ii}=-3.8$, $\zeta_i=2.0$; for Co 3*d*, $H_{ii}=-9.7$, $\zeta_{i1}=5.55$, $c_1=0.558$, $\zeta_{i2}=1.9$; $c_2=0.668$; for P 3*s*, $H_{ii}=-18.6$, $\zeta_i=1.84$; for P 3*p*, $H_{ii}=-14.0$, $\zeta_i=1.45$. This calculation closely reproduces a previously reported one, but we extract the partial density of states curves to demonstrate the procedure for fitting the experimental valence band spectra.[16]

III. RESULTS AND DISCUSSION

A. High-resolution Sb 3*d* and P 2*p* spectra

Figure 2 shows the Sb 3*d* spectra for $\mathrm{LaFe_4Sb_{12}}$, $\mathrm{CeFe_4Sb_{12}}$, and $\mathrm{CoSb_3}$, and the P 2*p* spectrum for $\mathrm{CoP_3}$. Although the most fundamental use of XPS spectra is to correlate binding energies with oxidation states, its application to intermetallic compounds has not been widespread and greater difficulties are faced in trying to find reference compounds for comparison. The error for XPS binding energies is typically ±0.1 eV.

In $\mathrm{CoP_3}$, the P $2p_{3/2}$ binding energy of 129.3 eV is markedly lower than that in elemental phosphorus (130.0 eV),[41] and on a scale recently developed for a series of transition-metal monophosphides *M*P,[37] it corresponds to the presence of anionic phosphorus with an approximate charge of −1.0. From charge neutrality, this implies a charge of +3.0 on the Co atoms. Although these charges agree fortuitously with the simple ionic model proposed earlier, care must be exercised in interpreting these charges too literally, as cautioned elsewhere.[26]

In the antimonides, the Sb $3d_{5/2}$ binding energies of 528.0 eV for both $\mathrm{LaFe_4Sb_{12}}$ and $\mathrm{CeFe_4Sb_{12}}$ and 528.1 eV for $\mathrm{CoSb_3}$ are only slightly lower than that in elemental antimony (528.2 eV).[41] A comparison to binding energies in other Sb-containing compounds[41] suggests Sb charges of −0.4 in $\mathrm{LaFe_4Sb_{12}}$ and $\mathrm{CeFe_4Sb_{12}}$, and −0.1 in $\mathrm{CoSb_3}$. Again, from charge neutrality, this implies charges of +0.4 for the Fe atoms in $\mathrm{LaFe_4Sb_{12}}$ and $\mathrm{CeFe_4Sb_{12}}$ (assuming R^{3+}), and +0.3 for the Co atoms in $\mathrm{CoSb_3}$. These observations reflect the greater covalent character of the bonding that would be expected from reduced electronegativity differences in the antimonides.[42] If we start from an ionic picture containing Sb^{1-} and then allow covalent bonding to occur, donation of electron density from filled Sb orbitals to empty metal orbitals tends to increase shielding of the metal nuclear charge

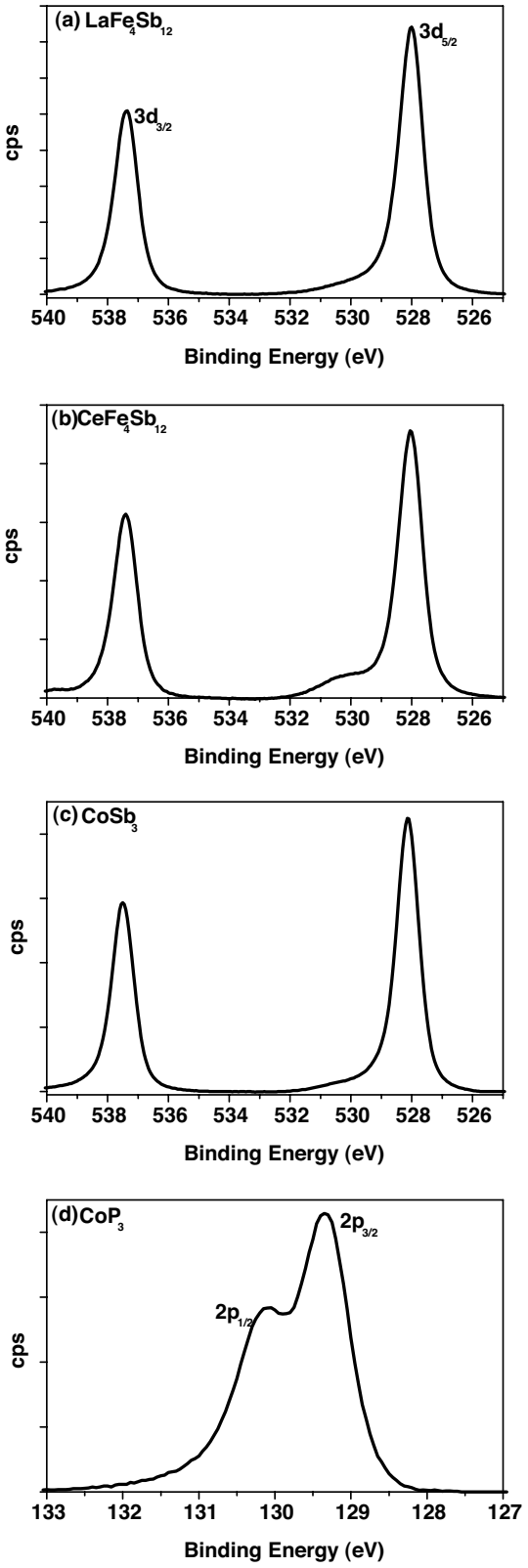

FIG. 2. High-resolution Sb 3*d* spectra of (a) $\mathrm{LaFe_4Sb_{12}}$, (b) $\mathrm{CeFe_4Sb_{12}}$, (c) $\mathrm{CoSb_3}$, and (d) P 2*p* spectrum of $\mathrm{CoP_3}$. The small satellite peak located above the Sb $3d_{5/2}$ core line is attributed to the presence of a small amount of Sb oxide not removed during sputtering. A small concentration of unreacted P centered near 130.6 eV was also observed in the P 2*p* spectrum from $\mathrm{CoP_3}$.

and decrease shielding of the Sb nuclear charge, which results in an Sb $3d_{5/2}$ binding energy that is only slightly less than that of elemental Sb.

B. High-resolution Fe and Co 2*p* spectra

Figure 3 shows the Fe $2p$ spectra for $LaFe_4Sb_{12}$ and $CeFe_4Sb_{12}$, and the Co $2p$ spectra for $CoSb_3$ and CoP_3. The observation of only one set of $2p_{3/2}$ and $2p_{1/2}$ signals indicates a single valence state, and the sharpness of these peaks along with the absence of multiplet splitting indicates a low-spin state for the metal atoms. This is consistent with proposals for the presence of only low-spin Fe^{2+} or Co^{3+} ($t_{2g}^6 e_g^0$). The asymmetry of both the $2p_{3/2}$ and $2p_{1/2}$ peaks in these spectra is an interesting feature that we have previously observed for $LaFe_4P_{12}$ and $CeFe_4P_{12}$.[23] According to a process described by Doniach and Šunjić, the asymmetric tail arises from the scattering of valence electrons between a continuum of states below and above the Fermi edge.[43] Typically this process is observed in metals where metal-metal bonding occurs, but other sources of delocalization, such as that between the metal and pnicogen atoms, which appear in these compounds, can also give rise to the asymmetric line shape.

The Fe $2p_{3/2}$ binding enegies of 706.7 eV for $LaFe_4Sb_{12}$ and 706.8 eV for $CeFe_4Sb_{12}$ are lower than in the phosphide analogues $LaFe_4P_{12}$ and $CeFe_4P_{12}$ (707.2 eV) and are essentially the same as that in Fe metal (706.8 eV).[41] The Co $2p_{3/2}$ binding energies of 778.1 eV for $CoSb_3$ and 778.5 eV for CoP_3 can be compared to that in Co metal (778.1 eV).[37,41] These comparisons illustrate the greater covalent character in the antimonides than in the phosphides, but the shifts in metal binding energy appear to be less sensitive to a change in the bonding character than in the pnicogen binding energy (Sec. III A). Nevertheless, the trends in the binding energy correlations with charge remain self-consistent whether the metal or pnicogen atoms are examined; for example, the greater positive Co charge found in CoP_3 compared to $CoSb_3$ can be inferred from either the Co or *Pn* binding energies.

A curious observation first noted by Anno *et al.*[17] in the XPS spectra for binary skutterudites ($CoSb_3$, $CoAs_3$) is that the energy separation between the metal $2p_{1/2}$ and $2p_{3/2}$ peaks seems to be remarkably similar to that of the metal (Co), as is the case here. Normally, the energy separation between spin-orbit doublets can be assumed to be proportional to Z (atomic number) and $1/r^3$ (r=radius).[44] Although the splittings in the Fe $2p$ (13 eV) and Co $2p$ peaks (15 eV) differ through the effect of Z, further differences arising from changes in charge, and thus r, do not seem to be manifested. This may be the result of delocalization of the valence electrons on the metal, which is also the cause of the asymmetric line shape. An alternative explanation suggests that the splitting in the core levels can be enhanced through coupling with stronger crystal field effects on the metal $3d$ band.[45] The observed splittings are also similar to those in clean metal surfaces (Fe, 13.2 eV; Co, 14.9 eV). It appears that these crystal field interactions are small to a degree that they do not separate the $2p$ doublets any more than in the elemental metals.

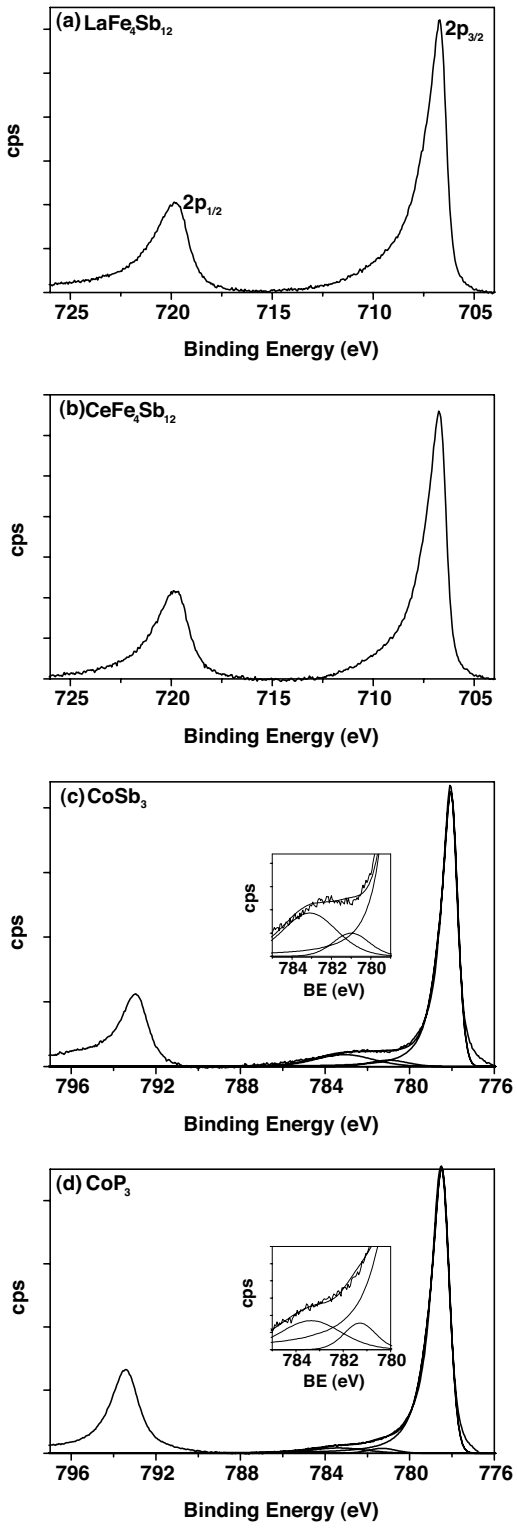

FIG. 3. High-resolution Fe $2p$ spectra of (a) $LaFe_4Sb_{12}$ and (b) $CeFe_4Sb_{12}$; and Co $2p$ spectra of (c) $CoSb_3$ and (d) CoP_3. The insets in (c) and (d) show the satellite peaks observed above the Co $2p_{3/2}$ peaks for $CoSb_3$ and CoP_3.

C. Co 2*p* satellite structure

Distinct satellite peaks at higher binding energy than the core lines are observed in the Co 2*p* spectra of $CoSb_3$ and CoP_3, being especially visible for the $2p_{3/2}$ signal, as shown in the insets of Figs. 3(c) and 3(d). These satellites have also been observed previously in the spectra of Co metal and CoP, and after additional REELS analysis on Co metal, an explanation involving plasmon loss instead of a two-core-hole theory was proposed.[37] Below we reconsider each of the models to account for the satellite structure in $CoSb_3$ and CoP_3, and demonstrate that useful chemical information can be extracted from its analysis.

Plasmon loss occurs when a photoelectron, after being ejected from an atom, is inelastically scattered by valence electrons of other atoms located close to its path as it travels to the surface of the solid. This interaction causes the valence electrons to oscillate, with the energy required to begin this oscillation being removed from the photoelectron.[46] Because the photoelectron has a lower kinetic energy, it is manifested as a satellite peak in the XPS spectrum with an apparently higher binding energy than the main core line. As in Co metal, the appearance of two satellite peaks [Figs. 3(c) and 3(d)] can then be assigned to bulk (higher binding energy) and surface plasmon loss (lower binding energy).[37] It should be noted that plasmon loss has also been observed to occur in Ni, Cr, and Fe.[47–49] The Ni and Cr analysis was carried out using EELS,[47,48] whereas plasmon loss in Fe was observed by analysis of the 1*s* XPS core line using a high energy Cu *K* x-ray source.[49] The Fe $2p_{3/2}$ peaks for RFe_4Sb_{12} presented in Figs. 3(a) and 3(b) do not show the presence of a plasmon loss peak, likely because the loss structure is overlapped by the Fe $2p_{1/2}$ peak.[49]

The two-core-hole theory was first introduced by Kotani and Toyozawa to account for the low intensity, high binding energy satellite peaks present in La 3*d* spectra[50] and later to those in Co and Ni as well.[51–53] This theory suggests that, after photoionization, the core hole present within an atom can influence the conduction states, causing them to be pulled below the Fermi edge (E_F). If the state pulled below E_F is empty, then a poorly screened final state is produced containing two holes: one within the core level and one within the valence band, the latter accounting for the observed satellite peak. If the state pulled below E_F contains an electron, then a well screened final state is produced in which excess energy is surrendered to the outgoing electron, giving it a higher kinetic energy (and an apparently lower binding energy).[53] This final state appears as the strong core line [$2p_{3/2}$ or $2p_{1/2}$ in the case of the Co spectra in Figs. 3(c) and 3(d)].

In the spectra of CoP_3 or $CoSb_3$, the main $2p_{3/2}$ satellite peak is separated from the core line by ~5 eV, as is the case for CoP or Co metal. In the two-core-hole theory, the amount of energy given to the photoelectron by the filled conduction state as it is lowered below E_F should depend on the energy gap between the valence and conduction bands. The satellite location for Co and CoP, which are metals,[54] should then be different from that for CoP_3 and $CoSb_3$, which are small band gap semiconductors.[8] On the other hand, in the plasmon loss model, the valence electrons of the Co atoms are all located close to E_F and would require similar amounts of energy to initiate plasmon oscillation, regardless of the compound. Thus, the invariance of the satellite location observed experimentally argues strongly for the plasmon loss model.

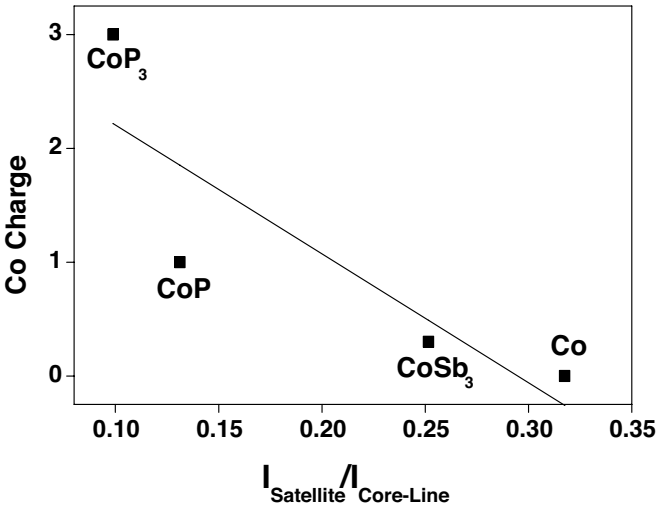

FIG. 4. Correlation between Co charge and relative intensity of the Co 2*p* satellite in Co, $CoSb_3$, CoP, and CoP_3. The data for Co and CoP are from Ref. 37.

Both models predict that the intensity of the satellite peak will depend on the occupancy of the metal valence states. In the plasmon loss model, the cross-section for plasmon oscillation events will increase if there are more valence electrons. In the two-core-hole theory, the cross-section for the production of a two-core-hole state will also increase with more valence electrons; this poorly screened state, which accounts for the satellite peak, is stabilized as the occupancy of the valence states increases.

The relationship between satellite intensity and electron population can be verified. Earlier we inferred charges on the Co atoms in CoP_3 and $CoSb_3$ from the pnicogen core-line binding energies. Figure 4 shows a plot of the Co charges in these and other solids versus the ratio of the total satellite intensity ($I_{satellite}$) over the core-line intensity ($I_{core\text{-}line}$) in the Co 2*p* spectra. The plot confirms that the presence of more valence electrons (lower positive charge) on the Co atoms correlates with a greater satellite intensity (higher $I_{satellite}/I_{core\text{-}line}$). It illustrates convincingly how covalency acts to arrive at true charges that are much less extreme than those based on oxidation state formalisms, and how delocalization of bonding electrons within the valence band becomes a significant factor on progressing to $CoSb_3$ given the similarity of its satellite intensity to Co metal.

D. High-resolution rare-earth 3*d* spectra

Figure 5 shows the La 3*d* spectrum for $LaFe_4Sb_{12}$ and the Ce 3*d* spectrum for $CeFe_4Sb_{12}$. Judged by their similarity to other reference spectra, including the phosphides $LaFe_4P_{12}$ and $CeFe_4P_{12}$,[23] they are consistent with the presence of trivalent *R*, a banal expectation for La compounds, but not so obvious for Ce compounds. The valence of cerium in skut-

terudites has been a source of debate,[26,34,35] but comparison with previously recorded spectra of CeF_3 and CeF_4 [Figs. 5(c) and 5(d)][23] shows conclusively that it is +3 in $CeFe_4Sb_{12}$, indicating the presence of a $4f^1$ state within the valence band.

At higher binding energy to the main $3d_{5/2}$ core line (A), these spectra reveal satellite peaks (B) that have previously been accounted for by a ligand-to-metal charge-transfer shake-up process.[23] After an atom is excited and the photoelectron ejected, the relaxation of the electrons in the atom as a result of their response to the presence of a core hole can precipitate a secondary process in which a valence electron on the ligand is also excited to empty conduction states localized on the rare earth.[55] The energy required to promote an electron from the ligand valence state to the empty conduction states on the rare earth is therefore not available to the photoelectron, causing it to appear in the spectrum with a higher binding energy (lower kinetic energy) than the core line. The empty $4f$ states are estimated to be 4–6 eV above the Fermi edge.[56] The satellite peaks shown in Fig. 5 are near this energy (2–4 eV), providing further support for the shake-up process. The cross-section for this process increases with greater overlap between ligand and rare-earth states, and with lower electronegativity of the ligand, allowing valence electrons to relax more readily from the ligand to the rare earth.[57] This is particularly evident in comparing the Ce $3d$ spectra, where the satellite intensity is more intense for $CeFe_4Sb_{12}$ than for $CeFe_4P_{12}$.[23]

Surprisingly, the opposite is true in the La $3d$ spectra of $LaFe_4Sb_{12}$ and $LaFe_4P_{12}$, but it is not immediately obvious why. Moreover, in addition to the shake-up satellite peak (B), there is another satellite peak (C) at lower binding energy to the main $3d_{5/2}$ core line [Fig. 5(a)] in $LaFe_4Sb_{12}$ that was not observed in $LaFe_4P_{12}$. Here, the two-core-hole model described earlier (Sec. III C) can be invoked as a plausible explanation for this additional satellite. The assumption of partial covalent character of the La-Sb bonds may allow for the presence of electrons in the La $4f$ states. If, after production of a core hole, a La conduction state containing an electron is pulled below E_F, then the La atom has a well screened final state in which this electron relinquishes its energy to the photoelectron. The photoelectron has an increased kinetic energy and appears below the core-line peak (A) on the binding energy scale. A similar satellite structure has been observed in the La $3d$ spectrum of LaSb and was also attributed to a two-core hole like process arising from partial filling of La $4f$ states.[58]

The separation from the core line to this new satellite peak (C) is ~2 eV, the same as that to the shake-up peak (B), which is reasonable because both peaks arise from movement of electrons across the band gap. The two-core-hole theory also offers the possibility for an empty La conduction state to be pulled below E_F, forming a poorly screened final state containing two holes (one within the core and one within the valence levels).[50] This final state leads to the generation of a photoelectron having a higher binding energy than the core line. Accordingly, yet another satellite peak (D) can be found between the $3d_{5/2}$ shake-up satellite and the $3d_{3/2}$ states in the spectrum of $LaFe_4Sb_{12}$ [Fig. 5(a)].

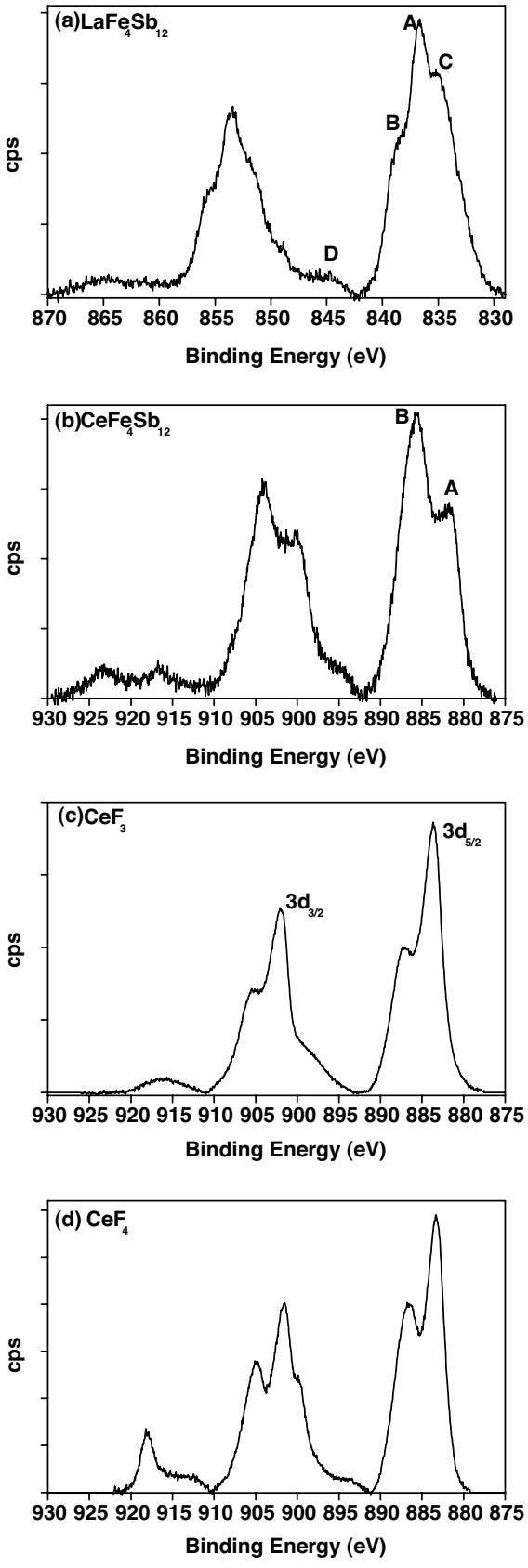

FIG. 5. High-resolution rare-earth $3d$ spectra of (a) $LaFe_4Sb_{12}$ and (b) $CeFe_4Sb_{12}$. The spectra for (c) CeF_3 and (d) CeF_4 are reproduced from Ref. 23.

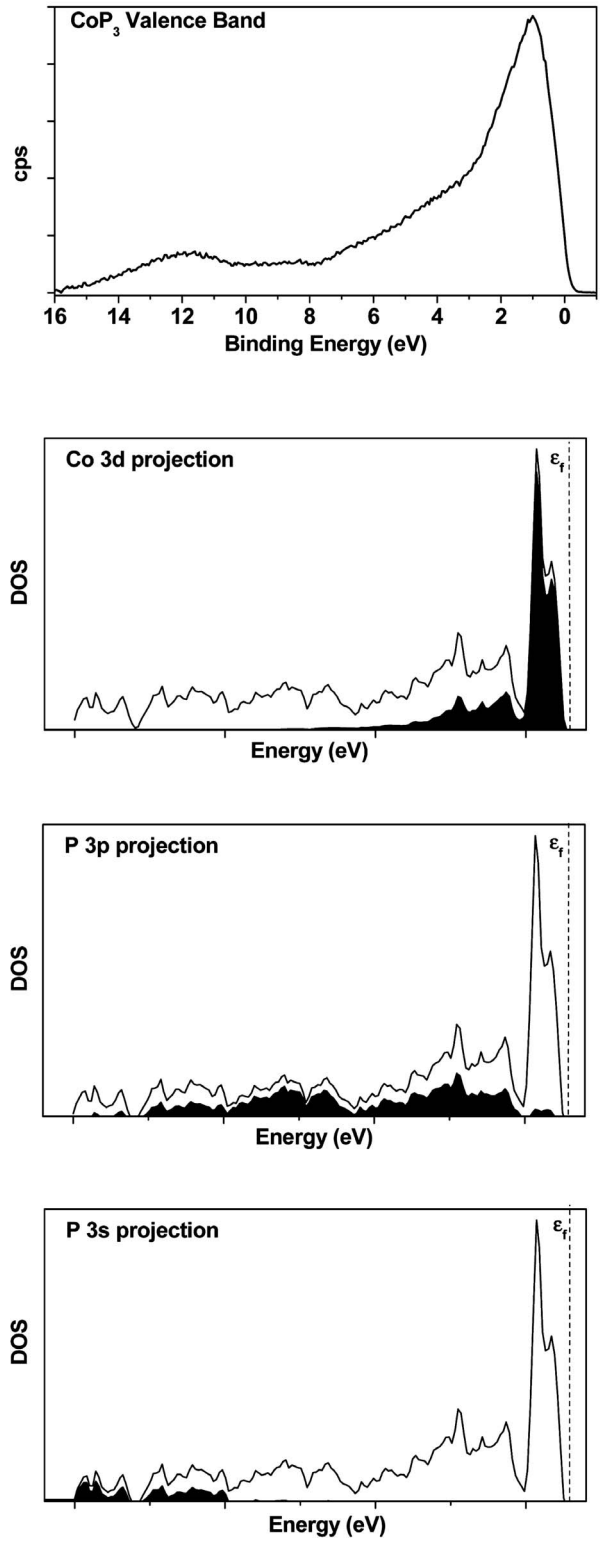

FIG. 6. Valence band spectrum of CoP_3 compared with the Co 3*d*, P 3*p*, and P 3*s* projections of the density of states. The Fermi edge (E_F) is indicated in each of the projections.

In contrast, the two-core-hole satellite structure is absent in the spectrum of $CeFe_4Sb_{12}$ [Fig. 5(b)]. If trivalent Ce is assumed, the $4f^1$ state may already be substantially involved in bonding states in the valence band below E_F, and as such would be unable to participate in two-core-hole processes.

Returning to the question of why the shake-up peak in the La 3*d* spectrum is more intense in $LaFe_4P_{12}$ than in $LaFe_4Sb_{12}$, we offer the simplest explanation that the two-core-hole and shake-up processes are competitive, given that both involve either the promotion or demotion of electrons across the band gap. With the La-P bond in $LaFe_4P_{12}$ probably having significant ionic character, the La 4*f* states do not mix well with the P states and remain essentially empty, so that only shake-up processes are likely to occur.

E. Valence band spectra

Although theoretical band structures determined using more rigorous methods (e.g., DFT, LMTO) are now available for many skutterudites,[11–16,18–20,26,27,30] we reproduce here the results of a simple calculation on CoP_3 that suffices to illustrate how the experimental valence band spectra can be fitted to component states.[16] Figure 6 shows that the observed valence band spectrum of CoP_3 matches very well to the calculated density of states (DOS) curve. As assigned from the projections of the DOS curve, the spectrum shows a P 3*s* band at high binding energy, followed by a very broad P 3*p* band that ends well before E_F, and an intense narrow Co 3*d* band just below E_F. Analysis of overlap population curves (not shown) indicates that Co-P bonding occurs throughout the upper portion of the valence band whereas P-P bonding occurs in the lower portion of the valence band.

Figure 7 shows the valence band spectra for $CoSb_3$, CoP_3, $LaFe_4Sb_{12}$, and $CeFe_4Sb_{12}$, fitted on the basis of the assignments above, through a methodology that we have applied elsewhere to phosphides.[23,37] The $CoSb_3$ spectrum compares well to those previously reported.[17,18] In general, the valence band in the antimonide skutterudites ($CoSb_3$, $LaFe_4Sb_{12}$, $CeFe_4Sb_{12}$) is not as wide as in the corresponding phosphides (CoP_3, $LaFe_4P_{12}$, $CeFe_4P_{12}$),[23] in agreement, for example, with calculations on $CeFe_4Sb_{12}$ and $CeFe_4P_{12}$.[26] In the spectra of the antimonides, the Sb 5*s* states occur in the lower portion of the valence band but both Sb 5*p* and Fe 3*d* states are clustered together in the upper portion of the valence band. The difference between the spectra of $LaFe_4Sb_{12}$ and $CeFe_4Sb_{12}$ is difficult to detect, but if they are overlaid (Fig. 8), a higher intensity is apparent near 2 eV in the case of $CeFe_4Sb_{12}$. We interpret this feature as arising from the presence of a Ce $4f^1$ state, at an energy similar to that found in $CeFe_4P_{12}$ (2.5–2.8 eV) (Refs. 23 and 36) and in agreement with density functional calculations which locate it near E_F just below the top of the Fe 3*d* band.[26]

Table I lists the binding energies and FWHM of the component peaks used to fit the valence band spectra. The asymmetric lower region was fitted by two pnicogen *ns* peaks, and correspondingly the upper region of the valence band was fitted by two pnicogen *np* peaks, which overlap with the transition-metal $3d_{5/2}$ and $3d_{3/2}$ spin-orbit doublet peaks placed at the edge closest to E_F. The asymmetry of the *Pn ns* peak may be caused by the presence of *Pn-Pn* bonds of differing length[2,3] as well as the overlap of *Pn-Pn* and metal-*Pn* states. The spectrum of CoP_3 shows additional intensity in the region between the P 3*s* and lower binding energy P

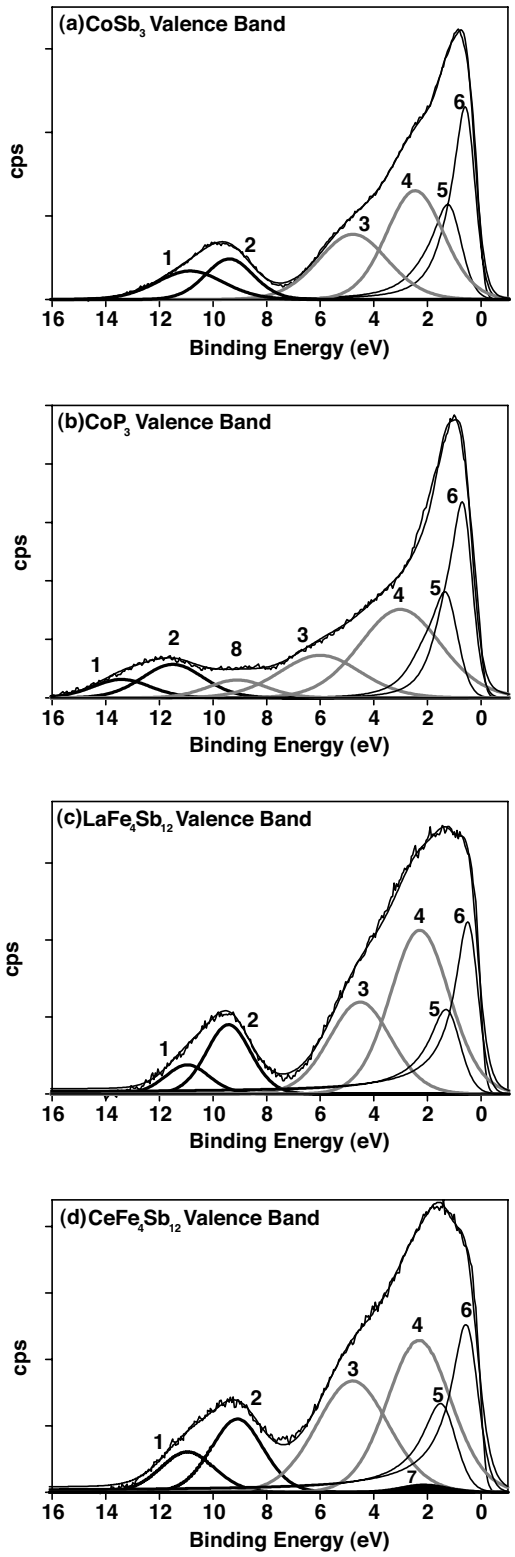

FIG. 7. Fitted valence band spectra of (a) $CoSb_3$, (b) CoP_3, (c) $LaFe_4Sb_{12}$, and (d) $CeFe_4Sb_{12}$. The identity, energies, and FWHM of the peaks used to fit the spectra are shown in Table I. The thick black lines represent *Pn ns* peaks, the thick gray lines represent *Pn np* peaks, and the thin black asymmetric lines represent the *M* $3d_{3/2,5/2}$ peaks. The Ce $4f$ state in $CeFe_4Sb_{12}$ is represented by a filled black peak centered at ~2 eV.

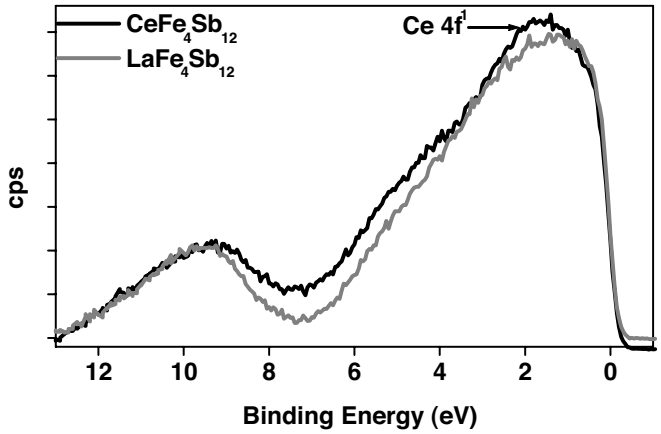

FIG. 8. Overlapped valence band spectra of $LaFe_4Sb_{12}$ and $CeFe_4Sb_{12}$ showing the position of the Ce $4f^1$ state.

$3p$ peaks, requiring a third P $3p$ peak to properly fit this region. In the spectrum of $CeFe_4Sb_{12}$, a Ce $4f$ peak was centered at ~2 eV.

The electron populations of the component states in the fitted valence band spectra can be determined from the peak intensities I_i, corrected for different photoionization cross-sections (σ) and inelastic mean free paths (IMFP, λ) (Table II), and normalized to give a fractional electron concentration C_i according to: $C_i=[I_i/(\sigma_i\lambda_i)]/[\Sigma_{j=1}^{n} I_j/(\sigma_j\lambda_j)]$.[59] Multiplying C_i by the total number of valence electrons (24 for $CoSb_3$, CoP_3; 95 for $LaFe_4Sb_{12}$; 96 for $CeFe_4Sb_{12}$) gives the number of electrons in each state, from which atomic charges can be deduced (Table III). Not only does this partitioning process of the electron populations provide further support for trivalent Ce in $CeFe_4Sb_{12}$, it also reproduces the familiar charges predicted from simple electron counting models, viz., the expectation of Co^{3+} and Fe^{2+} species (d^6), and anionic Pn^{1-}. These values are consistent with the results determined earlier from analysis of the core-line spectra, which tends to give charges that are less extreme but more discriminated. For example, whereas Sb charges of −0.4 for RFe_4Sb_{12} and −0.1 for $CoSb_3$ result from analysis of the Sb $3d$ core-line spectra, they are all found to be −1.0 from analysis of the valence band spectra. The core-line analysis is more sensitive to true differences in covalency in individual bonds to a given atom.

TABLE I. Binding energies (eV) of component peaks in valence band spectra of $CoSb_3$, CoP_3, $LaFe_4Sb_{12}$, and $CeFe_4Sb_{12}$. FWHM values (eV) are indicated in parentheses.

Peak	Assignment	$CoSb_3$	CoP_3	$LaFe_4Sb_{12}$	$CeFe_4Sb_{12}$
1	*Pn ns A*	10.9 (2.9)	13.4 (2.5)	11.0 (1.9)	10.9 (2.3)
2	*Pn ns B*	9.4 (2.1)	11.5 (2.7)	9.4 (2.0)	9.1 (2.3)
3	*Pn* $np_{3/2}$ *A*	4.8 (3.1)	6.0 (3.6)	4.5 (2.7)	4.8 (3.2)
4	*Pn* $np_{3/2}$ *B*	2.5 (2.5)	3.0 (3.6)	2.3 (2.6)	2.3 (2.8)
5	*M* $3d_{3/2}$	1.2 (1.2)	1.3 (1.1)	1.3 (1.2)	1.5 (1.3)
6	*M* $3d_{5/2}$	0.6 (0.9)	0.7 (0.9)	0.5 (0.9)	0.6 (1.1)
7	Ce $4f_{7/2}$				2.1 (2.0)
8	*Pn* $np_{3/2}$ *C*		9.1 (2.6)		

TABLE II. Corrections applied to peak intensities in valence band spectra of CoP_3, $CoSb_3$, $LaFe_4Sb_{12}$, and $CeFe_4Sb_{12}$. The P $3p_{3/2}$ cross-sections were corrected on the basis of comparison of experimental cross-sections determined by Brillson and Ceasar[60] to those calculated by Scofield.[61] All other cross-sections listed are those calculated by Scofield.[61] These cross-sections were determined for an excitation energy equal to that of Al Kα x rays.[61] The IMFP values were determined using the QUASES™ IMFP calculator and a kinetic energy of 1485 eV (Ref. 62). These values are calculated assuming that the material only contains the element of interest and are considered estimates when applied to materials containing multiple elements in the simple calculation presented here.

Atom	State	Photoionization cross-section [σ]	IMFP [λ] (Å)
Ce	$4f_{7/2}$	0.078	25.1
Co	$3d_{3/2}$	0.1082	24.0
	$3d_{5/2}$	0.1582	
Fe	$3d_{3/2}$	0.0694	25.9
	$3d_{5/2}$	0.1017	
P	$3s_{1/2}$	0.1116	33.9
	$3p_{3/2}$	0.0708	
Sb	$5s_{1/2}$	0.1085	30.4
	$5p_{3/2}$	0.0747	

IV. CONCLUSION

The measured XPS spectra of $LaFe_4Sb_{12}$, $CeFe_4Sb_{12}$, $CoSb_3$, and CoP_3 has provided insights into their electronic structure. High-resolution core-line spectra of the pnicogen atoms confirmed that the decrease in electronegativity from P to Sb produces a shift of binding energy that reflects the lower ionicity of bonds to these atoms. Such a shift is less apparent in the metal $2p$ spectra, where delocalization of electron density tends to temper effects on the shielding of the nuclear charge and also induces a strong peak asymmetry. A plasmon loss satellite peak is observed in the Co $2p$ spectra of these and other Co compounds whose relative intensity increases as the Co $3d$ band occupancy increases. This interesting relationship may serve as a broader basis for quantifying Co charges on other Co-containing compounds. The presence of trivalent R was confirmed in the RFe_4Sb_{12} compounds, as was determined previously in the phosphide analogues. The La $3d$ spectrum of $LaFe_4Sb_{12}$ contains two types of satellite peaks, arising from ligand-to-metal charge-transfer shake-up and from two-core-hole processes, both of which are final state effects whereby electrons are promoted from or demoted to states in the valence band. In contrast, only a shake-up satellite peak is found in the Ce $3d$ spectrum of $CeFe_4Sb_{12}$; a two-core-hole process is thwarted by the presence of a Ce $4f^1$ state in the valence band involved in bonding, so that no electrons are available in $4f$ states above E_F that can undergo this process. Neither is the two-core-hole process active in the phosphide $LaFe_4P_{12}$ because the La-P bonds are too ionic to allow conduction electrons to populate La $4f$ states. Fitting of the valence band spectra supports the formulations $(Co^{3+})(Pn^{1-})_3$ and $(R^{3+})(Fe^{2+})_4(Sb^{1-})_{12}$ (electronically balanced by a hole in the valence band), consistent with previous electrical, magnetic and Mössbauer measurements, and with theoretical models. The presence of Ce^{3+} in $CeFe_4Sb_{12}$ was confirmed by a $4f$ peak at ~2 eV in the valence band spectrum, but this observation was more difficult to make than in the previous case of $CeFe_4P_{12}$ because it is obscured by the greater mixing of states in the more covalent antimonide.

TABLE III. Electron populations in $CoSb_3$, CoP_3, $LaFe_4Sb_{12}$, and $CeFe_4Sb_{12}$. The La charge was assumed from analysis of the La $3d$ high-resolution spectrum.

State	$CoSb_3$	CoP_3	$LaFe_4Sb_{12}$	$CeFe_4Sb_{12}$
Pn ns A	1.8	0.9	3.4	4.9
Pn ns B	1.8	1.7	8.2	8.6
Pn np A	6.1	4.5	22.1	26.6
Pn np B	8.4	9.3	38.0	32.1
Pn np C		1.3		
M $3d$	5.9	6.3	23.2	22.5
Ce $4f$				1.3
Total number of e^-	24	24	95	96
Calculated charge per atom	+3.1 (Co), −1.0 (Sb)	+2.7 (Co), −0.9 (P)	+3 (La), +2.2 (Fe), −1.0 (Sb)	+2.7 (Ce), +2.4 (Fe), −1.0 (Sb)

ACKNOWLEDGMENTS

The Natural Sciences and Engineering Research Council (NSERC) of Canada supported this work through Discovery Grants to R.G.C. and A.M. Access to the Kratos XPS was kindly provided by the Alberta Centre for Surface Engineering and Science (ACSES) at the University of Alberta. ACSES was created with capital funding from the Canada Foundation for Innovation (CFI), which also provides interim operating support, and Alberta Innovation and Science. A.P.G. thanks the NSERC and the University of Alberta for support.

*Author to whom correspondence should be addressed. Electronic address: andrew.grosvenor@ualberta.ca

[1] I. Oftedal, Z. Kristallogr. **66**, 517 (1928).
[2] S. Rundqvist and N.-O. Errson, Ark. Kemi **30**, 103 (1968).
[3] W. Jeitschko and D. Braun, Acta Crystallogr., Sect. B: Struct. Crystallogr. Cryst. Chem. **33**, 3401 (1977).
[4] D. J. Braun and W. Jeitschko, J. Solid State Chem. **32**, 357 (1980).

[5] D. J. Braun and W. Jeitschko, J. Less-Common Met. **72**, 147 (1980).
[6] G. A. Slack, in *CRC Handbook of Thermoelectrics*, edited by D. M. Rowe (CRC Press, Boca Raton, 1995), p. 407.
[7] B. C. Sales, D. Mandrus, B. C. Chakoumakos, V. Keppens, and J. R. Thompson, Phys. Rev. B **56**, 15081 (1997).
[8] G. S. Nolas, D. T. Morelli, and T. M. Tritt, Annu. Rev. Mater. Sci. **29**, 89 (1999).
[9] B. C. Sales, in *Handbook on the Physics and Chemistry of Rare Earths*, edited by K. A. Gschneidner, Jr., J.-C. G. Bünzli, and V. K. Pecharsky (Elsevier, Amsterdam, 2003), Vol. 33, p. 1.
[10] J. Ackermann and A. Wold, J. Phys. Chem. Solids **38**, 1013 (1977).
[11] D. Jung, M.-H. Whangbo, and S. Alvarez, Inorg. Chem. **29**, 2252 (1990).
[12] D. J. Singh and W. E. Pickett, Phys. Rev. B **50**, 11235 (1994).
[13] M. Llunell, P. Alemany, S. Alvarez, V. P. Zhukov, and A. Vernes, Phys. Rev. B **53**, 10605 (1996).
[14] J. O. Sofo and G. D. Mahan, Phys. Rev. B **58**, 15620 (1998).
[15] M. Fornari and D. J. Singh, Phys. Rev. B **59**, 9722 (1999).
[16] M. Partik and H. D. Lutz, Phys. Chem. Miner. **27**, 41 (1999).
[17] H. Anno, K. Matsubara, T. Caillat, and J.-P. Fleurial, Phys. Rev. B **62**, 10737 (2000).
[18] I. Lefebvre-Devos, M. Lassalle, X. Wallart, J. Olivier-Fourcade, L. Monconduit, and J. C. Jumas, Phys. Rev. B **63**, 125110 (2001).
[19] E. Z. Kurmaev, A. Moewes, I. R. Shein, L. D. Finkelstein, A. L. Ivanovskii, and H. Anno, J. Phys.: Condens. Matter **16**, 979 (2004).
[20] K. Koga, K. Akai, K. Oshiro, and M. Matsuura, Phys. Rev. B **71**, 155119 (2005).
[21] F. Grandjean, A. Gérard, D. J. Braun, and W. Jeitschko, J. Phys. Chem. Solids **45**, 877 (1984).
[22] G. J. Long, D. Hautot, F. Grandjean, D. T. Morelli, and G. P. Meisner, Phys. Rev. B **60**, 7410 (1999).
[23] A. P. Grosvenor, R. G. Cavell, and A. Mar, Chem. Mater. **18**, 1650 (2006).
[24] D. T. Morelli and G. P. Meisner, J. Appl. Phys. **77**, 3777 (1995).
[25] M. E. Danebrock, C. B. H. Evers, and W. Jeitschko, J. Phys. Chem. Solids **57**, 381 (1996).
[26] L. Nördstrom and D. J. Singh, Phys. Rev. B **53**, 1103 (1996).
[27] D. J. Singh and I. I. Mazin, Phys. Rev. B **56**, R1650 (1997).
[28] D. J. Gajewski, N. R. Dilley, E. D. Bauer, E. J. Freeman, R. Chau, M. B. Maple, D. Mandrus, B. C. Sales, and A. H. Lacerda, J. Phys.: Condens. Matter **10**, 6973 (1998).
[29] D. Ravot, U. Lafont, L. Chapon, J. C. Tedenac, and A. Mauger, J. Alloys Compd. **323-324**, 389 (2001).
[30] H. Harima and K. Takegahara, Physica B **328**, 26 (2003).
[31] R. Viennois, D. Ravot, F. Terki, C. Hernandez, S. Charar, P. Haen, S. Paschen, and F. Steglich, J. Magn. Magn. Mater. **272-276**, e113 (2004).
[32] E. D. Bauer, R. Chau, N. R. Dilley, M. B. Maple, D. Mandrus, and B. C. Sales, J. Phys.: Condens. Matter **12**, 1261 (2000).
[33] R. Viennois, S. Charar, D. Ravot, P. Haen, A. Mauger, A. Bentien, S. Paschen, and F. Steglich, Eur. Phys. J. B **46**, 257 (2005).
[34] J. S. Xue, M. R. Antonio, W. T. White, L. Soderholm, and S. M. Kauzlarich, J. Alloys Compd. **207/208**, 161 (1994).
[35] F. Grandjean, G. J. Long, R. Cortes, D. T. Morelli, and G. P. Meisner, Phys. Rev. B **62**, 12569 (2000).
[36] H. Ishii, T. Miyahara, Y. Takayama, K. Obu, M. Shinoda, C. Lee, H. Shiozawa, S. Yuasa, T. D. Matsuda, H. Sugawara, and H. Sato, Surf. Rev. Lett. **9**, 1257 (2002).
[37] A. P. Grosvenor, S. D. Wik, R. G. Cavell, and A. Mar, Inorg. Chem. **44**, 8988 (2005).
[38] N. Fairley, CasaXPS version 2.3.9, Casa Software Ltd., Teighnmouth, Devon, UK, 2003 (www.casaxps.com).
[39] M.-H. Whangbo and R. Hoffmann, J. Am. Chem. Soc. **100**, 6093 (1978).
[40] R. Hoffmann, *Solids and Surfaces: A Chemist's View of Bonding in Extended Structures* (VCH Publishers, New York, 1988).
[41] C. D. Wagner, A. V. Naumkin, A. Kraut-Vass, J. W. Allison, C. J. Powell, and J. R. Rumble, Jr., *NIST X-ray Photoelectron Spectroscopy Database*, version 3.4 (web version), National Institute of Standards and Technology, Gaithersburg, MD, 2003 (srdata.nist.gov/xps).
[42] A. L. Allred and E. G. Rochow, J. Inorg. Nucl. Chem. **5**, 264 (1958).
[43] S. Doniach and M. Šunjić, J. Phys. C **3**, 285 (1970).
[44] D. Briggs and J. C. Rivière, in *Practical Surface Analysis, Volume I—Auger and X-ray Photoelectron Spectroscopy*, edited by D. Briggs and M. P. Seah (Wiley, Chichester, 1990), p. 113.
[45] L. Ley, R. A. Pollak, F. R. McFeely, S. P. Kowalczyk, and D. A. Shirley, Phys. Rev. B **9**, 600 (1974).
[46] R. F. Egerton and M. Malac, J. Electron Spectrosc. Relat. Phenom. **143**, 43 (2005).
[47] H. A. E. Hagelin-Weaver, J. F. Weaver, G. B. Hoflund, and G. N. Salaita, J. Alloys Compd. **389**, 34 (2005).
[48] A. P. Grosvenor, M. C. Biesinger, R. St.-C. Smart, and N. S. McIntyre, Surf. Sci. **600**, 1771 (2006).
[49] N. Moslemzadeh, G. Beamson, P. Tsakiropoulos, and J. F. Watts, Surf. Sci. **600**, 265 (2006).
[50] A. Kotani and T. Toyozawa, J. Phys. Soc. Jpn. **37**, 912 (1974).
[51] S. Raaen, Solid State Commun. **60**, 991 (1986).
[52] S. Hüfner, *Photoelectron Spectroscopy* (Springer-Verlag, Berlin, 1995).
[53] H. W. Nesbitt, D. Legrand, and G. M. Bancroft, Phys. Chem. Miner. **27**, 357 (2000).
[54] F. Hulliger, Struct. Bonding (Berlin) **4**, 83 (1968).
[55] S. Imada and T. Jo, J. Phys. Soc. Jpn. **58**, 402 (1989).
[56] K.-H. Park and S.-J. Oh, Phys. Rev. B **48**, 14833 (1993).
[57] D. D. Sarma, P. Vishnu Kamath, and C. N. R. Rao, Chem. Phys. **73**, 71 (1983).
[58] Y. Baer, R. Hauger, Ch. Zürcher, M. Campagna, and G. K. Wertheim, Phys. Rev. B **18**, 4433 (1978).
[59] J. F. Watts and J. Wolstenholme, *An Introduction to Surface Analysis by XPS and AES* (Wiley, Rexdale, 2003).
[60] L. J. Brillson and G. P. Ceasar, Surf. Sci. **58**, 457 (1976).
[61] J. H. Scofield, J. Electron Spectrosc. Relat. Phenom. **8**, 129 (1976).
[62] S. Tougaard, QUASES-IMFP-TPP2M: Database for Calculation of IMFPs by TPP2M Formula, version 2.1, QUASES-Tougaard Inc., Odense, Denmark, 2000 (www.quases.com).